Can Tho University Journal of Science
website: sj.ctu.edu.vn

DOI: 10.22144/ctu.jen.2020.015

Al_2TiO_5/SBA-15 promoting photocatalytic degradation of cinnamic acid

Nguyen Dien Trung[2], Nguyen Thanh Nhuan[2], Mai Van Hieu[1] and Nguyen Thi Hong[1*]

[1]*College of Natural Sciences, Can Tho University*

[2]*School of Education, Can Tho University*

**Correspondence: Nguyen Thi Hong (email: nthong43@ctu.edu.vn)*

Article info.

Received 04 Mar 2020
Revised 13 Apr 2020
Accepted 31 Jul 2020

Keywords

Cinnamic acid, degradation, mesoporous silica material, photocatalyst, pseudobrookite

ABSTRACT

The synthesis of Al_2TiO_5/SBA-15 (ATO/SBA) catalysts was investigated by the sol-gel method using precursors including aluminum nitrate, titanium isopropoxide, SBA-15, and citric acid. The formation of ATO/SBA phases was analyzed by X-ray diffraction (XRD). The content of ATO in ATO/SBA catalysts strongly affected the photocatalytic degradation of cinnamic acid (CA). The obtained results showed that 75% ATO in ATO/SBA (75ATO/SBA) phases led to the highest efficiency of CA photodegradation. The characteristics of 75ATO/SBA sample were determined by Fourier transform infrared spectroscopy, Brunauer-Emmett-Teller adsorption, UV-Vis diffuse reflectance spectroscopy, and transmission electron microscopy. Moreover, the activity of 75ATO/SBA on photocatalytic degradation of CA was also investigated by catalyst dosage, initial pH of CA solution, and airflow rate. The optimum condition for photodegradation efficiency of CA was found to be at C_{cat} = 0.75 g/L, pH = 3.8, Q_{air} = 0.3 L/min and t_{react} = 6 hrs.

Cited as: Trung, N.D., Nhuan, N.T., Hieu, M.V. and Hong, N.T., 2020. Al_2TiO_5/SBA-15 promoting photocatalytic degradation of cinnamic acid. Can Tho University Journal of Science. 12(2): 45-52.

1 INTRODUCTION

Nowadays, water pollution has been considered as a disastrous consequence of the rapid development in agriculture and industry. Organic materials consisting of organic dyes (Assémian *et al.*, 2018), phenolic acids (Madureira *et al.*, 2018), surfactants (Wu *et al.*, 2019), pesticides (Dutta *et al.*, 2015), and personal care pharmaceuticals (Rovani *et al.*, 2014) were directly disposed to water that contaminated both surface and groundwater. These polluted compounds in water were difficult to eliminate owing to low concentrations and high persistence in the natural environment. The recycling of wastewater was considered considered powerful to sovle the problem of water shortage. Practically, various strategies including physical and biological methods were proposed to meet the demand for organic wastewater treatment. However, the efficiency of degradation fell short of expectation due to the incomplete oxidation of organic pollutants and time-consuming for the treatment process. Thus, oxidation methods such as ozonation, Fenton oxidation, photocatalytic oxidation, supercritical water oxidation, and the electrochemical method which offered high-efficiency degradation of polluting compounds were widely used to treat wastewater (Khin *et al.*, 2012; Brillas *et al.*, 2015). Among these, photocatalytic oxidation offered high efficiency and low cost in the process of wastewater regeneration. Photocatalysis was able

to mineralize the persistent organics to carbon dioxide, water, and inorganic acids at room temperature. In the presence of oxygen along with light irradiation, electrons, and holes of semiconductor catalysts triggered the formation of radicals ($OH^{\bullet}$ and $O_2^{\bullet-}$) which subsequently oxidized organic materials in wastewater (Malik *et al.*, 2015).

It has been reported that pseudobrookite-type oxide Al_2TiO_5 (ATO) offered photocatalytic activities on the degradation of waste organic material. Especially, ATO is effective to eliminate pollutants in the wastewater. However, the main disadvantage of ATO is a low surface area (21.1 m^2/g) which is unfavorable to the initial adsorption of reactants in photodegradation (Bakhshandeh *et al.*, 2018). In order to enhance the surface area of ATO, mesoporous silica SBA-15 (SBA) with a uniform, mesopore diameter (9.1–16.7 nm), high surface area (609–777 m^2/g), and high pore volume (0.92–1.65 cm^3/g) is added to the ATO as a catalyst-host (Dos Santos *et al.*, 2013).

The principal objective of the present research is to synthesize a porous host-material Al_2TiO_5/SBA-15 (ATO/SBA) and analyze photochemical properties. The influence of SBA loading in hybridization has been demonstrated by the photocatalytic activity towards the cinnamic acid (CA) degradation under UV irradiation. In this work, CA was selected as a decompositional model of the phenolic acid. The CA removal was evaluated by operational factors such as catalyst dosages, initial solution pH, and airflow rates. Furthermore, reusability and stability of photocatalyst were also investigated at optimal conditions for the CA removal.

2 EXPERIMENTS

2.1 Materials

Pluronic P-123 ($EO_{20}PO_{70}EO_{20}$, Sigma-Aldrich, M_n = 5,800), tetraethyl orthosilicate ($(C_2H_5O)_4Si$, Sigma-Aldrich, 98.0%) and hydrochloric acid (HCl, Prolabo, 98.0%) were used to prepare silica material SBA. Aluminum nitrate nonahydrate ($Al(NO_3)_3{\cdot}9H_2O$, Xilong, 99.7%), ethanol absolute (C_2H_6O, Xilong, 95.0%), monohydrate citric acid ($C_6H_8O_7{\cdot}H_2O$, Sigma-Aldrich, 99.5%) and titanium isopropoxide ($Ti(OC_3H_7)_4$, Sigma-Aldrich, 97.0%) used to synthesize ATO/SBA catalysts. Cinnamic acid ($C_9H_8O_2$, Sigma-Aldrich, 97.0%) was used to study photocatalytic degradation. Sodium chloride (NaCl, Sigma-Aldrich, 99.0%) and sodium hydroxide (NaOH, Sigma-Aldrich, 97.0%) were used for adjusting solution pH.

2.2 Synthesis of catalyst

2.2.1 Preparation of SBA

Silica material SBA was synthesized based on the procedure in reported literature (Aranda, *et al.*, 2010). Four grams of pluronic P-123 was first dissolved in distilled water and stirred for 2 hrs to form a homogeneous solution. Secondly, 8.52 g of $(C_2H_5O)_4Si$ and 24 mL of HCl were added to the pluronic P-123 solution. The obtained mixture solution was hydrolyzed by autoclave at 60°C for 24 hrs to produce a white precipitate. After washing and drying to remove impurities, the precipitate was annealed at 550ºC for 10 hrs to obtain silica material SBA.

2.2.2 Preparation of ATO/SBA catalysts

ATO/SBA catalysts were synthesized by the sol-gel approach. The ATO solution was prepared by mixing 3.75 g of $Al(NO_3)_3{\cdot}9H_2O$, 2.10 g of $C_6H_8O_7{\cdot}H_2O$, 5 mL of C_2H_5OH and 3 mL of $Ti(OC_3H_7)_4$. A specific amount of silica material SBA was added to the ATO solution, and then the mixture solution was stirred for 1 hr to form an identical gel. After drying at 60°C for 24 hrs, the ATO/SBA gel was calcined at 700°C with a heating rate of 10°C/min for 3 hrs to obtain ATO/SBA catalysts. In these experiments, the mass percentages of ATO in the ATO/SBA catalyst were studied at 60, 70, 75, 80, and 90%. The corresponding catalysts were denoted as 60ATO/SBA, 70ATO/SBA, 75ATO/SBA, 80ATO/SBA, and 90ATO/SBA, respectively.

2.3 Characteristics of catalyst

X-ray diffraction (XRD) patterns of ATO/SBA catalysts were recorded on Bruker D2 Pharser X-Ray Diffractometer with Cu Kα radiation in 2θ = 10–80º. In the case of SBA, XRD patterns were recorded on Bruker D8 Pharser X-Ray Diffractometer in 2θ = 0.5–10º. Nitrogen adsorption-desorption isotherms were determined by using a Nova 2200e instrument. The specific surface area of catalysts was calculated according to the Brunauer-Emmett-Teller (BET) nitrogen adsorption isotherms. The morphology and surface properties of materials were investigated by Jeol Jem 7401 scanning electron microscope (SEM) and Jeol Jem 1400 transmission electron microscopy (TEM) apparatuses. Fourier transform infrared spectroscopy (FTIR) measurements were used for the charac-

teristics of functional groups and recorded in the range from 400 to 4000 cm^{-1}. UV-Vis diffuse reflectance spectroscopy (DRS) was used to examine the bandgap of the catalysts and recorded on a Varian Cary 5000 UV-Vis-NIR spectrophotometer with an integrating sphere in the range of 200−800 nm.

2.4 Photocatalytic activity of the catalyst

The photocatalytic activity of catalysts was studied by the degradation of 50 mg/L CA solution at room temperature and atmospheric pressure. The reaction mixture of ATO/SBA and CA was stirred in the dark for 40 mins to establish the adsorption/desorption equilibrium before exposure to the UV light irradiation of 36 UVA Engin LZ1-00U600 lamps (λ = 350–400 nm with the maximum peak at 365 nm). The entire process of decomposition lasted 6 hrs. The influence of catalyst dosage, initial solution pH, and airflow rate on the photoactivity of ATO/SBA catalyst with the highest CA removal was investigated in detail. The reaction solution was separated by filtration and analyzed the obtained CA solution by a UV-visible spectrophotometer on UV-1800 (Shimadzu) at 272 nm. CA solution was removed at the end of each batch and replaced by a fresh CA solution to conduct the photocatalytic reactions in succession. The stability of catalysts was tested at the optimized conditions until CA conversion decreased at 30%.

3 RESULTS AND DISCUSSION

The small-angle XRD patterns of SBA materials were illustrated in Figure 1. The main peak at value 2θ of 0.95°, and two smaller peaks placed at 1.58° and 1.84° were typical for mesoporous materials and hexagonal structure corresponding to (100), (110), and (200) planes of SBA (Thielemann *et al.*, 2011). It can be concluded that SBA material was successfully synthesized.

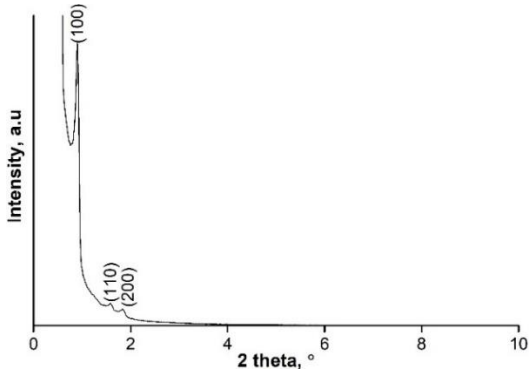

Fig. 1: The small-angle XRD pattern of SBA

The XRD patterns of ATO/SBA catalysts with different ATO loadings from 60 to 90% were presented in Figure 2. All catalysts consisted of the peaks at 18.9, 26.6, 33.7, 38.0, 42.0, 47.7, 50.7, 54.1, 57.0, 58.3, and 62.4° which was assigned to ATO phases (Keyvani *et al.*, 2019). A minor peak at 25.2° was identified to anatase TiO_2 as well as SiO_2 (Azarniya *et al.*, 2015; Yao *et al.*, 2015). The obtained results showed that ATO phases were maintained and the intensity of the SiO_2 phase increased with a higher loading of SBA. It means that there was the formation of ATO and SBA phase in the synthesized catalysts.

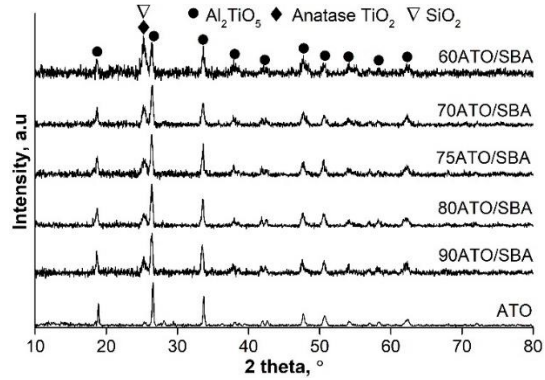

Fig. 2: XRD pattern of ATO/SBA catalysts

The effect of CA degradation for 360 mins in the photocatalytic reaction on the obtained ATO/SBA catalysts was shown in Figure 3. The amount of ATO in hybrid catalysts significantly affected their photocatalytic activity for CA removal. The 360-minute conversion percentage (X_{360}) slightly rose from 62.2% to 80.2% with an increase of ATO content in ATO/SBA catalysts from 60% to 75% and decreased with a further increase of ATO content. The highest photocatalytic activity toward CA elimination at 75% of ATO in ATO/SBA catalysts might relate to high dispersion between ATO and SBA to form more active sites. The decrease of CA degradation efficiency at higher 75% ATO loadings was due to the decrease in pores which absorb CA from solution (Li *et al.*, 2016; Phan *et al.*, 2018). According to the obtained results, 75ATO/SBA catalyst was chosen as the optimum materials in the present study.

The FTIR spectra of the 75ATO/SBA catalyst was measured in the range of 400–4000 cm^{-1} (Figure 4). A broad peak appeared at 3423 cm^{-1} was to stretch vibrations of OH groups while the peak at 1645 cm^{-1} was assigned for the scissor bending vibration of O–H (Mojet *et al.*, 2010). The peaks at 463, 806, and 1080 cm^{-1} were attributed to Si–O

asymmetric stretching. On the other hand, a peak at 930 cm^{-1} belonged to Si–OH vibration (Jin *et al.*, 2013; Zeng *et al.*, 2013). These results agreed with the XRD analysis in which the obtained materials comprised both SBA and ATO.

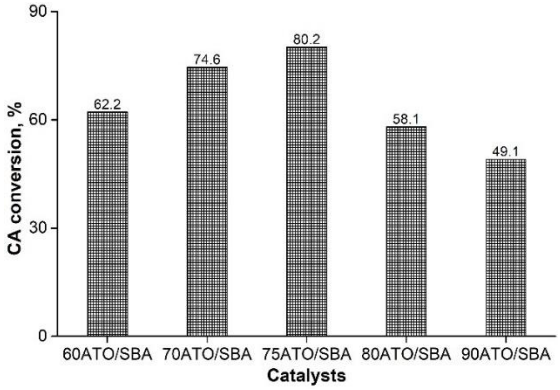

Fig. 3: The CA degradation for 360 mins in the photocatalytic reaction on ATO/SBA catalysts at pH = 3.8, C_{cat} = 0.75 g/L, Q_{air} = 0.3 L/min, and T = 25 ºC

Table 1: The bandgap energy E_g and the absorbable wavelength λ of catalysts: ATO and 75ATO/SBA

Catalyst	E_g (eV)	λ (nm)
ATO	3.18	390
75ATO/SBA	3.42	363

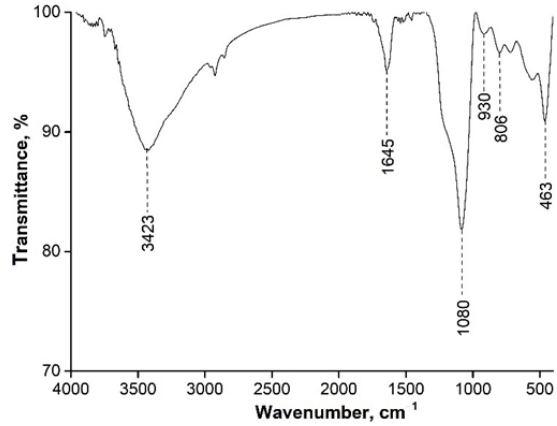

Fig. 4: FTIR spectra of 75ATO/SBA catalyst

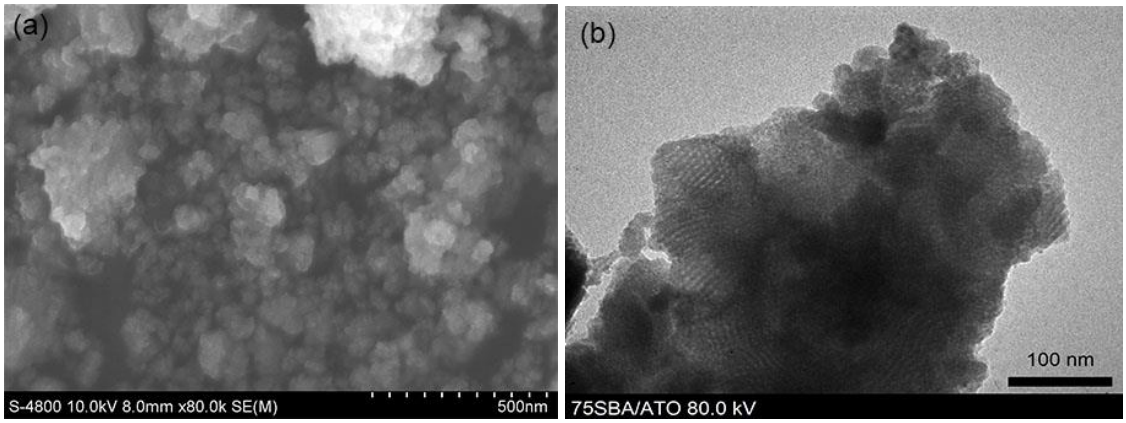

Fig. 5: SEM (a) and TEM (b) images of 75ATO/SBA catalyst

The SEM and TEM images of the 75ATO/SBA catalyst were shown in Figure 5. There was the appearance of quasi-sphere-like nanoparticles with various channels related to the aggregation of ATO/SBA particles (Figure 5a). The particle sizes ranged from 30 to 50 nm. ATO with the particle size of 20 nm was observed on the pore channels of SBA, which elucidated that ATO was present in nanoparticle form and well-dispersed on the mesoporous structure of SBA (Figure 5b).

Figure 6a demonstrated the DRS spectra of catalysts: ATO and 75ATO/SBA. The bandgap energy of ATO and 75ATO/SBA catalysts calculated by the Tauc plot (Figure 6b) reached 3.18 and 3.42 eV, respectively. Two catalysts also absorbed wavelengths in the UV light (Table 1).

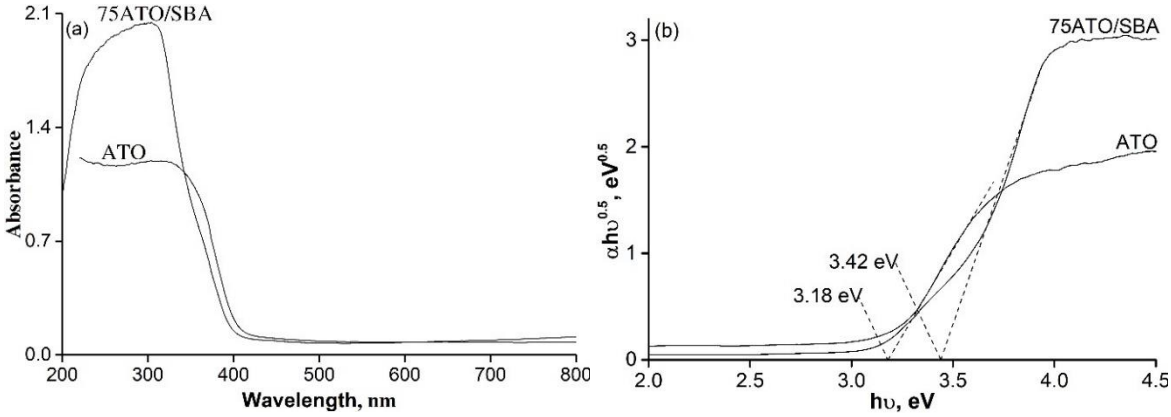

Fig. 6: UV-Vis diffuse reflectance spectra (a) and Tauc plot (b) of ATO/SBA catalysts

Table 2: The specific surface area S_{BET}, the pore size d_{pore}, and the pore volume V_{pore} of catalysts: ATO and ATO/SBA

Catalyst	S_{BET} (m^2/g)	d_{pore} (nm)	V_{pore} (mL/g)
ATO	26.8	2.2	0.028
75ATO/SBA	149.3	2.2	0.151

The nitrogen adsorption-desorption isotherms of ATO and ATO/SBA catalysts were shown in Figure 7. Two catalysts were typical type IV isotherms mesoporous materials with type H1 hysteresis (Bardestani *et al.*, 2019). Especially, the surface area and pore volume of the 75ATO/SBA catalyst were much higher than that of a single ATO catalyst (Table 2).

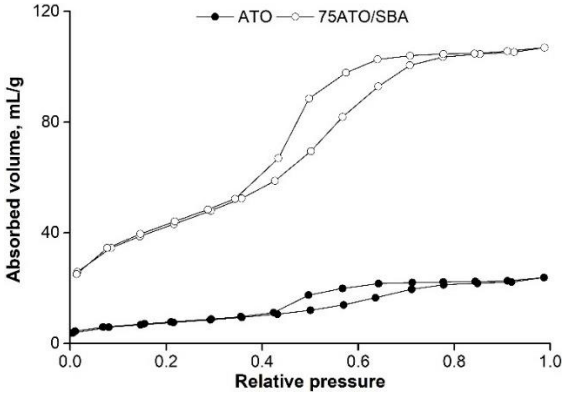

Fig. 7: Nitrogen adsorption-desorption isotherms on ATO and 75ATO/SBA catalyst

The influence of the operational parameters on the photoactivity in CA degradation was determined on 75ATO/SBA catalyst. The effect of catalyst dosage on CA removal was studied by varying amounts of catalysts in the range of 0.50–1.25 g/L while the effect of reaction time was tested in the range of 30-360 min. The obtained results were shown in Figure 8, the conversion percentage of CA was significantly affected by the catalyst dosages and reaction time. The conversion percentage of CA steadily increased with an increase of reaction time with any catalyst dosages. The percentage of CA removal strongly increased from 50 to 80.2% after the 360-min reaction with an increase of catalyst dosage from 0.5 g/L to 0.75 g/L and slightly decreased with a further increase of catalyst dosage. The increase in the amount of catalyst led to an increase of active sites on the catalyst surface, which in turns formed more hydroxyl radicals to initiate the decomposition reaction (Kalantary *et al.*, 2015). When the amount of the catalyst was higher than the optimum value, a considerable reduction in the activity of the catalyst may link to the transmission of UV light through suspension (Georgaki *et al.*, 2014). According to the obtained results, 0.75 g/L of 75ATO/SBA catalyst was suggested as the optimum condition for CA removal.

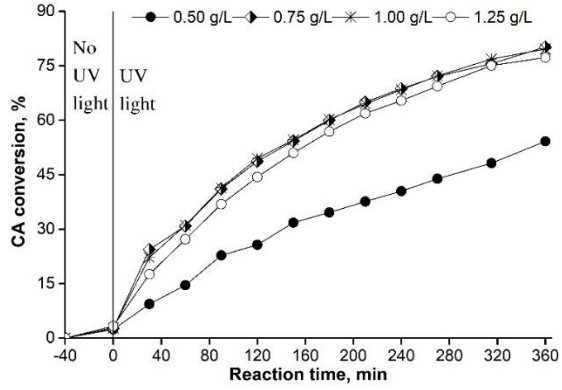

Fig. 8: The effect of the catalyst dosage on the photocatalytic degradation of CA on the 75ATO/SBA catalyst

It has been reported that the airflow rate primarily affected the activity of the photochemical catalyst. Therefore, the effect of air flow rate on the photocatalytic degradation of CA by 75ATO/SBA catalyst was studied in the range of 0-0.4 L/min in the present study. The obtained results were shown in Figure 9. The conversion percentage of CA slightly rose to 80.2% when the airflow rate increased from 0 to 0.3 L/min. There is a slight decrease in CA conversion with an increase in the airflow rate from 0.3 to 0.4 L/min. In the photocatalytic reaction, oxygen acted as an electron capture agent to prolong the recombination time of the photogenerated electrons with holes and simultaneously generate superoxide radicals (Reddy *et al.*, 2018). On the contrary, the higher oxygen flow rate may hinder the transmission of light into the catalyst (Lam *et al.*, 2010). This is the reason why the conversion percentage of CA decreased at a higher 0.3 L/min of the oxygen flow rate.

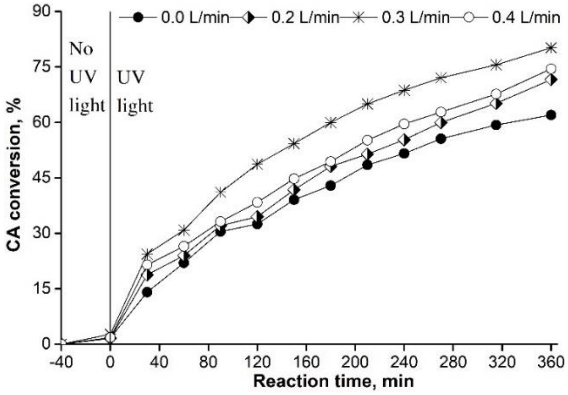

Fig. 9: The effect of the airflow rate on the photocatalytic degradation of CA on the 75ATO/SBA catalyst

The pH was acknowledged as an important parameter affecting the adsorption process on the surface charge of the catalyst. The effect of the initial pH on the CA removal was exhibited in Figure 10. The highest conversion percentage of CA was found to be at pH 3.8. At lower or higher pH 3.8, the CA conversion was not high. The observed phenomenon was due to the nature of the CA molecule and initial adsorption of CA on the catalyst surface. According to Pirilä *et al.* (2015), phenolic compound exhibited the best-degraded ability at low pH. Similar results were found in the study of Madureira *et al.* (2018) for the degradation of phenolic acids. The formation of radicals reduced in a strong acid medium. Meanwhile, the pH nature of phenolic compounds favored elimination thanks to the increased yields for the formation of radicals.

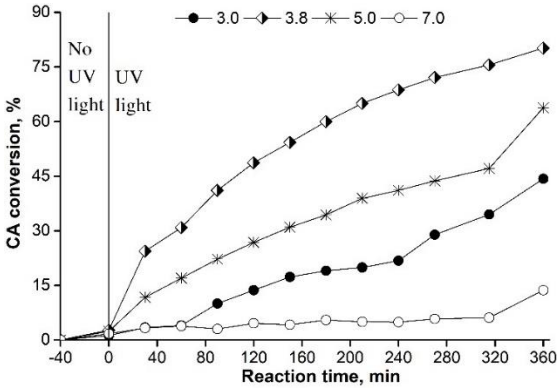

Fig. 10: The effect of the initial pH solution on the photocatalytic degradation of CA on the 75ATO/SBA catalyst

The reusability and stability of photocatalyst played an essential role in practical applications. In this study, the stability of 75ATO/SBA catalyst in optimal conditions including catalyst concentration at 0.75 g/L, airflow rate of 0.3 L/min, and initial pH of 3.8 was measured for 360 min from continuous cycles (Figure 11). It was clear that a slight decrease in CA degradation was observed in each cycle. Under similar experimental conditions, the CA removal decreased about 33%: X_{360} = 79.6% at the first cycle compared to X_{360} = 53.4% in the sixth cycle. The reduction of 75ATO/SBA photocatalyst to eliminate CA could be explained by the precipitation of the CA degraded sediments on the catalyst, which may potentially block active sites on the surface (Kakavandi *et al.*, 2019).

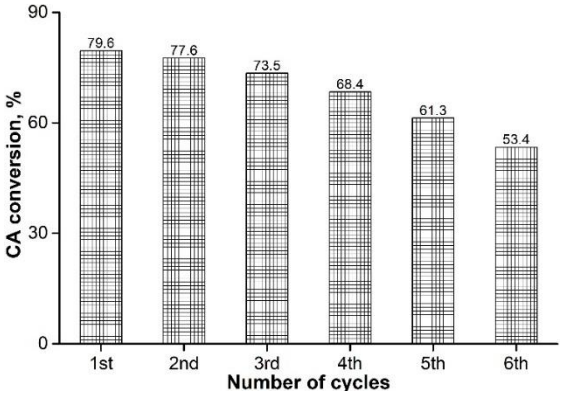

Fig. 11: Reusable 75ATO/SBA catalyst for CA degradation

The difference in the photocatalytic activity and photochemical characteristics of 75ATO/SBA

compared to the ATO catalyst as illustrated in Figure 12. In comparison with the ATO catalyst, there was a modest variation in CA conversion on 75ATO/SBA catalyst. X_{360} of 75ATO/SBA catalyst was slightly lower than that of the ATO catalyst. Although the addition of SBA to ATO was favorable to the development of the surface area (with the 5.6-fold rise), an upsurge of the bandgap energy occurred on 75ATO/SBA. Thus, the lower activity of 75ATO/SBA catalysts in the CA elimination could be explained by increasing the value of the bandgap energy.

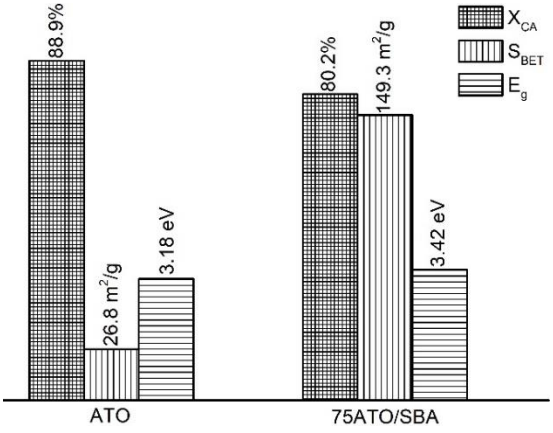

Fig. 12: The photocatalytic degradation and characteristics of catalysts: ATO and 75ATO/SBA

4 CONCLUSIONS

A series of ATO/SBA catalysts was successfully synthesized by the sol-gel technique. From the investigation of photocatalytic activity, it can be concluded 75ATO/SBA effectively degraded CA in photocatalytic conditions. The surface area of photocatalyst remarkably increased in the presence of SBA. The maximum conversion of CA was achieved at the optimum conditions: catalyst dosage of 0.75 g/L, the airflow rate of 0.3 L/min, and initial pH of 3.8 for 50 mg/L of CA after the 360-minute reaction. After six cycles, CA conversion remained more than 50%, which indicated that 75ATO/SBA was a good catalyst for recyclability and durability. Thus, 75ATO/SBA can be applied as a promising heterogeneous photocatalyst for the efficient degradation of organic pollutants.

ACKNOWLEDGMENTS

This work was supported by a grant from Can Tho University, Vietnam. The authors would like to thank for the financial support.

REFERENCES

Aranda, A., Puértolas, B., Solsona, B., *et al*., 2010. Total oxidation of naphthalene using mesoporous CeO_2 catalysts synthesized by nanocasting from two dimensional SBA-15 and three dimensional KIT-6 and MCM-48 silica templates. Catalysis Letters. 134(1): 110-117.

Assémian, A.S., Kouassi, K.E., Drogui, P., Adouby, K. and Boa, D., 2018. Removal of a persistent dye in aqueous solutions by electrocoagulation process: Modeling and optimization through response surface methodology. Water, Air, & Soil Pollution. 229(6): 184.

Azarniya, A., Azarniya, A., Hosseini, H.R.M. and Simchi, A., 2015. Nanostructured aluminium titanate (Al_2TiO_5) particles and nanofibers: Synthesis and mechanism of microstructural evolution. Materials Characterization. 103: 125-132.

Bakhshandeh, F., Azarniya, A., Madaah Hosseini H.R. and Jafari S., 2018. Are aluminum titanate-based nanostructures new photocatalytic materials? Possibilities and perspectives. Journal of Photochemistry and Photobiology A: Chemistry. 353: 316-324.

Bardestani R., Patience G.S. and Kaliaguine S., 2019. Experimental methods in chemical engineering: specific surface area and pore size distribution measurements-BET, BJH, and DFT. The Canadian Journal of Chemical Engineering. 97(11): 2781-2791.

Brillas E. and Martínez-Huitle C.A., 2015. Decontamination of wastewaters containing synthetic organic dyes by electrochemical methods. An updated review. Applied Catalysis B: Environmental. 166-167: 603-643.

dos Santos S.M.L., Nogueira K.A.B., de Souza Gama M., Lima J.D.F., da Silva Júnior I.J. and de Azevedo D.C.S., 2013. Synthesis and characterization of ordered mesoporous silica (SBA-15 and SBA-16) for adsorption of biomolecules. Microporous and Mesoporous Materials. 180: 284-292.

Dutta A., Chakraborty I., Sarkar D. and Chakrabarti S., 2015. Sunlight-assisted photo-Fenton degradation of pesticide in wastewater: Ecotoxicological impact on Nostoc sp. Algae. Water, Air, & Soil Pollution. 226(12): 398.

Georgaki I., Vasilaki E. and Katsarakis N., 2014. A study on the degradation of carbamazepine and ibuprofen by TiO_2 and ZnO photocatalysis upon UV/Visible-light irradiation. American Journal of Analytical Chemistry. 05: 518-534.

Jin Q., Qu F., Jiang J., Dong Y., Guo W. and Lin H., 2013. A pH-sensitive controlled dual-drug release from meso-macroporous silica/multilayer-polyelectrolytes coated SBA-15 composites. Journal of Sol-Gel Science and Technology. 66(3): 466-471.

Kakavandi B., Takdastan A., Pourfadakari S., Ahmadmoazzam M. and Jorfi S., 2019. Heterogeneous cata-

lytic degradation of organic compounds using nanoscale zero-valent iron supported on kaolinite: Mechanism, kinetic and feasibility studies. Journal of the Taiwan Institute of Chemical Engineers. 96: 329-340.

Kalantary R.R., Dadban Shahamat Y., Farzadkia M., Esrafili A. and Asgharnia H., 2015. Photocatalytic degradation and mineralization of diazinon in aqueous solution using nano-TiO_2(Degussa, P25): kinetic and statistical analysis. Desalination and Water Treatment. 55(2): 555-563.

Keyvani N., Azarniya A., Hosseini H.R.M., Abedi M. and Moskovskikh D., 2019. Thermal stability and strain sensitivity of nanostructured aluminum titanate (Al_2TiO_5). Materials Chemistry and Physics. 223: 202-208.

Khin M.M., Nair A.S., Babu V.J., Murugan R. and Ramakrishna S., 2012. A review on nanomaterials for environmental remediation. Energy & Environmental Science. 5(8): 8075-8109.

Lam S.M., Sin J.C. and Mohamed A.R., 2010. Parameter effect on photocatalytic degradation of phenol using TiO_2-P25/activated carbon (AC). Korean Journal of Chemical Engineering. 27(4): 1109-1116.

Li H., Zhu J., Xiao P., Zhan Y., Lv K., Wu L. and Li M., 2016. On the mechanism of oxidative degradation of rhodamine B over $LaFeO_3$ catalysts supported on silica materials: Role of support. Microporous and Mesoporous Materials. 221: 159-166.

Madureira J., Barros L., Melo R., Cabo Verde S., Ferreira I.C.F.R. and Margaça F.M.A., 2018. Degradation of phenolic acids by gamma radiation as model compounds of cork wastewaters. Chemical Engineering Journal. 341: 227-237.

Malik R., Duhan S., Nehra S. and Rana P., 2015. Effect of annealing temperature on the photocatalytic performance of SnO_2 nanoflowers towards degradation of Rhodamine B. Advanced Science. 7: 448-456.

Mojet B.L., Ebbesen S.D. and Lefferts L., 2010. Light at the interface: the potential of attenuated total reflection infrared spectroscopy for understanding heterogeneous catalysis in water. Chemical Society Reviews. 39(12): 4643-4655.

Pirilä M., Saouabe M., Ojala S.,*et al*., 2015. Photocatalytic degradation of organic pollutants in wastewater. Topics in Catalysis. 58(14): 1085-1099.

Phan T.T.N., Nikoloski A.N., Bahri P.A. and Li D., 2018. Adsorption and photo-Fenton catalytic degradation of organic dyes over crystalline $LaFeO_3$-doped porous silica. RSC Advances. 8(63): 36181-36190.

Reddy C.V., Babu B., Reddy I.N. and Shim J., 2018. Synthesis and characterization of pure tetragonal ZrO_2 nanoparticles with enhanced photocatalytic activity. Ceramics International. 44(6): 6940-6948.

Rovani S., Censi M.T., Pedrotti S.L., Lima É.C., Cataluña R. and Fernandes A.N., 2014. Development of a new adsorbent from agro-industrial waste and its potential use in endocrine disruptor compound removal. Journal of Hazardous Materials. 271: 311-320.

Thielemann J.P., Girgsdies F., Schlögl R. and Hess C., 2011. Pore structure and surface area of silica SBA-15: influence of washing and scale-up. Beilstein Journal of Nanotechnology. 2: 110-118.

Wu Q., Zhao L., Song R. and Ma A., 2019. Research progress of surfactant biodegradation. IOP Conference Series: Earth and Environmental Science. 227: 052023.

Yao Q., Lu Z.H., Yang K., Chen X. and Zhu M., 2015. Ruthenium nanoparticles confined in SBA-15 as highly efficient catalyst for hydrolytic dehydrogenation of ammonia borane and hydrazine borane. Scientific Reports. 5(1): 15186.

Zeng J., He B., Lamb K., De Marco R., Shen P.K. and Jiang S.P., 2013. Phosphoric acid functionalized presintered meso-silica for high temperature proton exchange membrane fuel cells. Chemical Communications. 49(41): 4655-4657.